On the Structure of Al_2O_3 and Photoelectron Spectra of $Al_2O_2^-$ and $Al_2O_3^-$

Edet F. Archibong and Alain St-Amant*

Department of Chemistry, University of Ottawa, 10 Marie Curie, Ottawa, Ontario K1N 6N5, Canada

Received: September 14, 1998; In Final Form: December 2, 1998

Ab initio and density functional theory (DFT) calculations with the 6-311+G(2df) basis set have been performed on Al_2O_3, Al_2O_2, and their corresponding negative ions. A triplet ground state is predicted for the Al_2O_3 molecule and a doublet ground state for $Al_2O_3^-$. Both Al_2O_3 and its negative ion have a C_{2v} structure, which is a distorted form of the structure proposed in a recent report on negative ion photoelectron spectroscopy (PES) of $Al_xO_y^-$ ($x = 1-2$, $y = 1-5$) [*J. Chem. Phys.* **1997**, *106*, 1309]. Al_2O_2 and its negative ion have a planar (D_{2h}) rhombic structure. The adiabatic electron affinity calculated at the CCSD(T) level is 3.28 eV for Al_2O_3 and 1.81 eV for Al_2O_2 compared to the experimental values of 3.71 and 1.88 eV, respectively. The singlet−triplet (S−T) gap of 0.49 eV observed for Al_2O_2 in the PES experiment compares quite well with our computed value of 0.47 eV. Adiabatic electron detachment energies (AEDE) of the anions calculated at the CCSD(T) level and B3LYP harmonic vibrational frequencies (including isotopic frequency shifts) of the lowest energy structures of the neutral molecules are provided for future experimental studies on these species.

Introduction

Previous theoretical calculations[1,2] and matrix isolation studies[3,4] appeared to have established the structure of the Al_2O_3 molecule as a symmetric linear OAlOAlO ($D_{\infty h}$). Therefore, it attracted our attention when, in a recent publication on the anion photoelectron spectroscopy of $Al_xO_y^-$ ($x = 1-2$, $y = 1-5$), Wang and his associates[5] suggested an alternative structure for Al_2O_3. According to their report,[5] the photoelectron spectrum (PES) of $Al_2O_3^-$ measured at 193 nm photon energy displays three bands labeled X, A, and B at binding energies of 3.71, 4.32, and 4.9 eV, respectively. Analysis of the experimental data yields an adiabatic electron affinity of 3.71 eV for Al_2O_3, and the ground-state X-band is reported to exhibit a vibrational progression of 850 ± 80 cm^{-1}. The authors conclude that a singlet C_{2v} structure in which a terminal oxygen atom is attached to an Al of a rhombic Al_2O_2 moeity is likely to be the species observed in their photoelectron experiment.[5] The C_{2v} isomer is also proposed as a viable candidate for the gas-phase equilibrium structure of Al_2O_3. Apparently, this structure is not one of those investigated in previous work on the Al_2O_3 molecule.[3,4]

The $Al_2O_2^-$ species was also studied by Wang et al.[5] The existence of the rhombic D_{2h} isomer of Al_2O_2 in matrix isolation studies is somewhat controversial.[4,6−10] In fact, no matrix experiment has established the existence of the rhombic isomer unequivocally[4] despite evidence from theory that it is the lowest energy structure of the Al_2O_2 molecule.[2,11−13] On the other hand, linear AlOAlO has been observed and characterized in cryogenic matrix studies.[4] Comprehensive infrared studies of matrix-isolated Al_2O_2 and Al_2O_3 molecules may be found in the work of Andrews and co-workers,[4] as well as in the reports by Serebrennikov and his associates.[3,8,10] On the theoretical side, Nemukhin and Weinhold have carried out elaborate ab initio calculations on the Al_2O_2 and Al_2O_3 molecules.[2] Archibong and Sullivan also studied Al_2O_2 as part of a theoretical investigation of M_2O_2 (M = Al, Ga, In, Tl) systems.[13] In the recent anion photoelectron spectroscopy of $Al_2O_2^-$, the ground state of the Al_2O_2 molecule is confirmed[5] as ^1A_g (D_{2h}), in agreement with earlier theoretical results. The adiabatic electron affinity of Al_2O_2 is measured as 1.88 eV, and the lowest triplet excited state is located 0.49 eV above the ^1A_g (D_{2h}) ground state.[5]

We have been investigating the structures and properties of some group 13 metal oxides isolated in cryogenic matrices and in the gas phase.[14,15] The suggestion from the recent photoelectron experiment[5] that the Al_2O_3 molecule probably has a structure different from that of the established linear OAlOAlO ($D_{\infty h}$) form warrants further investigation. Consequently, in this work, the potential energy surface of $Al_2O_3^-$ is examined and that of neutral Al_2O_3 is revisited. Earlier theoretical studies reported only stationary points located on the singlet potential energy surface. The current work examines stationary points on the singlet and triplet potential energy surfaces and also considers the structure recently proposed by Wang and co-workers.[5] A similar study is carried out for $Al_2O_2^-$ and Al_2O_2. A cardinal objective of this study is to compare the experimental results with theoretical predictions. The relative energies, vibrational frequencies, and adiabatic detachment energies are computed for several stable isomers of these species. Comparisons are then made with a segment of results obtained from the experimental negative ion photoelectron spectroscopy of $Al_2O_3^-$ and $Al_2O_2^-$.[5]

Computational Methods

Geometries are fully optimized at the ab initio HF and MP2 levels and also at the B3LYP level using the 6-311+G(2df) one-particle basis set.[16] Harmonic vibrational frequencies are computed by analytic second derivative methods at the B3LYP level and the nature of the stationary points verified via their Hessian indices. By use of the MP2 and B3LYP geometries, relative energies and adiabatic detachment energies are calculated with coupled cluster singles and doubles including perturbational estimates of triple excitations [CCSD(T)]. The adiabatic detachment energies are computed as the difference in the total energies of the anions and the neutral species at their respective optimized geometries. For the MP2 and CCSD(T) calculations, only the valence electrons are correlated;

10.1021/jp983695n CCC: $18.00
Published on Web 02/11/1999

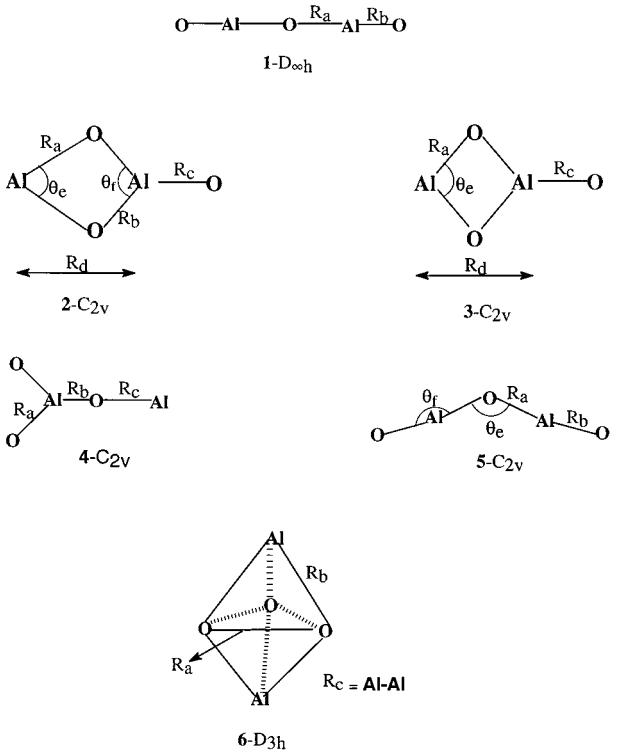

Figure 1. Structures of Al_2O_3 investigated in this work.

that is, we employed the frozen core (FC) approximation. The calculations are performed with GAUSSIAN 94.[17]

Results and Discussion

Previous ab initio calculations on the Al_2O_3 molecule have established the linear isomer, depicted as **1** in Figure 1, as the lowest energy stationary point on the singlet potential energy surface.[1,2] This isomer has also been identified from infrared studies of matrix-isolated Al + O_2 reaction products.[3,4] However, as stated in the Introduction, a singlet C_{2v} structure (depicted as **3**-C_{2v} in Figure 1) has been proposed, from photoelectron spectroscopy of $Al_2O_3^-$, as the likely gas-phase equilibrium structure of Al_2O_3.[5] It should be noted that a full geometry optimization within C_{2v} symmetry starting from **3** always results in the structure labeled **2**-C_{2v} in Figure 1. However, since **3**-C_{2v} is suggested as the species observed in the photoelectron experiments, the geometry has been constrained to remain at **3**. In the following section, we present the results of geometry optimizations and energies computed for several isomers of $Al_2O_3^-$ and Al_2O_3.

A. $Al_2O_3^-$ and Al_2O_3. First, we consider $Al_2O_3^-$. The structures optimized at the B3LYP and MP2 levels are sketched in Figure 1. The relative energies are listed in Table 1, and the geometrical parameters are included in Table 2. As noted above, the 6-311+G(2df) basis set is used for the calculations. The results in Table 1 indicate that the $^2A_1$ state of structure **3** (depicted as **3**-C_{2v} in Figure 1) is indeed more stable than **1**-$D_{\infty h}$ ($^2\Sigma_g^+$). At the B3LYP and MP2 levels, **3**-C_{2v} ($^2A_1$) is 1.48 and 1.57 eV, respectively, below **1**-$D_{\infty h}$ ($^2\Sigma_g^+$). In fact, a vibrational frequency analysis indicates that the linear form, **1**-$D_{\infty h}$ ($^2\Sigma_g^+$), is not a minimum energy structure and that it can distort to **5**-C_{2v} ($^2A_1$), a local minimum that lies roughly 0.30 eV below **1**. The most stable structure computed for $Al_2O_3^-$, however, is the **2**-C_{2v}. At the CCSD(T) level, the **2**-C_{2v} ($^2A_1$) structure lies roughly 0.11 eV (2.5 kcal/mol) below **3**-C_{2v} ($^2A_1$) and 1.37 eV below **5**-C_{2v} ($^2A_1$). Harmonic vibrational frequencies computed for **2**-C_{2v} ($^2A_1$) at the B3LYP level establish it as a minimum energy structure.

Next we consider neutral Al_2O_3. Earlier studies have ruled out several structures as possible candidates for the ground-state structure of Al_2O_3.[1,2] Some of these high-energy structures are not considered in the present work. The two isomers most pertinent to the present study, in addition to **1**, are **2**-C_{2v} and the closely related **3**-C_{2v} recently proposed for Al_2O_3. Table 1 lists the relative energies of these isomers at the B3LYP and MP2 levels. The results presented in this table show that the energetic ordering predicted for **1**−**3** at the MP2 level is quite different from that of B3LYP. The lowest energy structure computed at the MP2 level is **1**-$D_{\infty h}$ ($^1\Sigma_g^+$). The MP2 results suggest that the $^1A_1$ states of **2** and **3** are 0.84 and 1.31 eV, respectively, above the $^1\Sigma_g^+$ state of **1**, while the $^3B_2$ states of these C_{2v} structures are also less stable than the $^1\Sigma_g^+$ state by roughly 0.2 eV (4.6 kcal/mol). On the other hand, the B3LYP functional predicts a different energetic ordering. The $^1A_1$ states of **2** and **3** are 0.56 and 0.82 eV, respectively, above the $^1\Sigma_g^+$ state of **1**-$D_{\infty h}$, in qualitative agreement with the MP2 results. In contrast, B3LYP places the $^3B_2$ states of **2** and **3** roughly 0.3 eV (6.9 kcal/mol) below the $^1\Sigma_g^+$ (**1**-$D_{\infty h}$) state. It should be pointed out that spin contamination is not pronounced in the triplet calculations. $\langle S^2 \rangle$ does not exceed 2.01 at the UHF and UB3LYP levels for the $^3B_1$ and $^3B_2$ states of **2** and **3**.

The obvious discrepancy in the energetic orderings calculated at the MP2 and B3LYP levels for **1**-$D_{\infty h}$ ($^1\Sigma_g^+$) and the low-lying triplet states of **2** and **3** unfortunately complicates the definitive determination of the lowest energy structure of Al_2O_3. Consequently, additional calculations are performed within the coupled cluster approximation. By use of the CCSD(T)/6-311+G(2df) model, single-point energies are calculated for the $^1\Sigma_g^+$ (**1**-$D_{\infty h}$) state and three lowest states ($^1A_1$,$^3B_1$, and $^3B_2$) of **2**-C_{2v} using their optimized MP2 and B3LYP geometries, that is, CCSD(T)//MP2 and CCSD(T)//B3LYP energy calculations. The results of these calculations are included in Table 1. Both CCSD(T) results place the $^1A_1$ state of **2** at 0.7 eV (16 kcal/mol) above the $^1\Sigma_g^+$ state of **1**. However, the $^3B_1$ and $^3B_2$ states of **2** are computed to be 0.15 and 0.30 eV, respectively, below the $^1\Sigma_g^+$ state of **1**. It is obvious that the energy separation between $^1\Sigma_g^+$ (**1**-$D_{\infty h}$) and the low-lying triplet states of **2**-C_{2v} is not large. Nonetheless, the coupled cluster calculations predict $^3B_2$ (**2**-C_{2v}) to be more stable than $^1\Sigma_g^+$ (**1**-$D_{\infty h}$) by roughly 7 kcal/mol. The nearly identical energies calculated at the CCSD(T)//MP2 and CCSD(T)//B3LYP levels are not unexpected, since the geometrical parameters computed with MP2 and B3LYP for each species are very similar (see Table 2).

To arrive at a meaningful conclusion for the ground state of the Al_2O_3 molecule, we optimized the geometries of **1**-$D_{\infty h}$ ($^1\Sigma_g^+$) and **2**-C_{2v} ($^3B_2$) at the CCSD(T) level with the 6-31G(d) and 6-311G(d) basis sets followed by single-point energy calculations at the CCSD(T)/6-311+G(2df) level using the CCSD(T)/6-31G(d) and CCSD(T)/6-311G(d) geometries. The results of these calculations are also included in Tables 1 and 2. At the CCSD(T)/6-311G(d) level, **2**-C_{2v} ($^3B_2$) is found to be the ground state of Al_2O_3 with the linear isomer, **1**-$D_{\infty h}$ ($^1\Sigma_g^+$), 0.28 eV (6.4 kcal/mol) above. Further evidence that **2**-C_{2v} ($^3B_2$) is more stable than **1**-$D_{\infty h}$ ($^1\Sigma_g^+$) is obtained from a single-point energy calculation at the CCSD(T)/6-311+G(2df)//CCSD(T)/6-311G(d) level. The latter found **2**-C_{2v} ($^3B_2$) to be more stable than **1**-$D_{\infty h}$ ($^1\Sigma_g^+$) by 0.29 eV (6.7 kcal/mol). It is doubtful that geometry optimizations at a higher level of theory will significantly improve the quality of the results in Table 1. Therefore, on the basis of our CCSD(T) results, the ground state

TABLE 1: Relative Energies[a,b] (in eV) of Al_2O_3 and $Al_2O_3^-$ Computed Using the 6-311+G(2df) Basis Set

structure	state	MP2	B3LYP	CCSD(T)[c]	CCSD(T)[d]	CCSD(T)[e]	CCSD(T)[f]
				Al_2O_3			
1-$D_{\infty h}$	$^1\Sigma_g^+$	0.00	0.00	0.00	0.00	0.00	0.00
2-C_{2v}	$^1A_1$	0.84	0.56	0.70	0.69		
	$^3B_2$	0.22	−0.33	−0.30	−0.30	−0.30	−0.29
	$^3B_1$	0.36	−0.18	−0.15	−0.15		
3-C_{2v}	$^1A_1$	1.31	0.82	0.67			
	$^3B_2$	0.23	−0.32	−0.29	−0.29		
	$^3B_1$	0.37	−0.18				
4-C_{2v}	$^1A_1$	1.75	1.13				
5-C_{2v}		*g*	*g*				
6-D_{3h}	$^1A_1'$	2.09	1.92				
	$^3A_2'$	2.35	1.50				
				$Al_2O_3^-$			
1-$D_{\infty h}$	$^2\Sigma_g^+$	1.69	1.57				
2-C_{2v}	$^2A_1$	0.00	0.00	0.00	0.00		
	$^2B_2$	1.59	1.49				
	$^4B_2$	3.89	3.53				
	$^4B_1$	3.95	3.46				
3-C_{2v}	$^2A_1$	0.12	0.09	0.11	0.11		
	$^2B_2$	1.80	1.71				
4-C_{2v}	$^2B_1$	5.07	4.49				
5-C_{2v}	$^2A_1$	1.35	1.27	1.37			
6-D_{3h}	$^2A_1'$	2.41	2.21				

[a] Total energies (in hartrees) of Al_2O_3. For **1**-$D_{\infty h}$ ($^1\Sigma_g^+$): $E_{MP2} = -709.444\,733$; $E_{B3LYP} = -710.754\,541$; $E_{CCSD(T)//MP2} = -709.462\,831$; $E_{CCSD(T)//B3LYP} = -709.462\,886$. For **2**-$C_{2v}$($^3B_2$): $E_{MP2} = -709.436\,614$; $E_{B3LYP} = -710.766\,722$; $E_{CCSD(T)//MP2} = -709.473\,731$; $E_{CCSD(T)//B3LYP} = -709.473\,760$. For **3**-$C_{2v}$($^3B_2$) $E_{CCSD(T)//MP2} = -709.473\,500$; $E_{CCSD(T)//B3LYP} = -709.473\,505$. Total energies (in hartrees) of $Al_2O_3^-$. For **1**-$D_{\infty h}$ ($^2\Sigma_g^+$): $E_{MP2} = -709.507\,745$; $E_{B3LYP} = -710.832\,441$. For **2**-$C_{2v}$($^2A_1$): $E_{CCSD(T)//MP2} = -709.594\,136$; $E_{CCSD(T)//B3LYP} = -709.594\,187$. For **3**-$C_{2v}$($^2A_1$): $E_{CCSD(T)//MP2} = -709.590\,052$; $E_{CCSD(T)//B3LYP} = -709.590\,118$. [b] Corrections for zero-point energies are not included. [c] Computed at the MP2/6-311+G(2df) geometry. [d] Computed at the B3LYP/6-311+G(2df) geometry. [e] Computed at the CCSD(T)/6-31G(d) geometry [f] Computed at the CCSD(T)/6-311G(d) geometry; $E_{CCSD(T)/6-311G(d)}$ (**2**-$^3B_2$) − $E_{CCSD(T)/6-311G(d)}$ (**1**-$^1\Sigma_g^+$) = −0.28 eV. [g] Converged to **1**-$D_{\infty h}$ ($^1\Sigma_g^+$) on optimization.

of the Al_2O_3 molecule is the $^3B_2$ (**2**-C_{2v}) state. Above it are the $^3B_1$ (**2**-C_{2v}), $1\Sigma_g^+$ (**1**-$D_{\infty h}$) and $^1A_1$ (**2**-C_{2v}) states at 0.15, 0.29, and 1.00 eV, respectively.

It is disappointing, however, that our results do not agree well with the data[5] obtained from anion photoelectron spectroscopy of $Al_2O_3^-$. According to our calculations, the lowest state of $Al_2O_3^-$ is $^2A_1$ (**2**-C_{2v}) with valence electron configuration ... $(a_1)^2(b_2)^2(a_1)^2(a_1)^2(a_1)^2(b_2)^2(b_1)^2(b_2)^2(a_2)^2(a_1)^2(b_1)^2(b_2)^2(a_1)^1$. The energetic separation between the highest occupied molecular orbitals (MOs) is small, and the prediction of the relative energies of neutral states that may result from the detachment of an electron from these orbitals demands actual calculations. Photodetachment of an electron from the singly occupied a_1 bonding MO [significant contribution from Al (3s and $3p_z$) attached to two oxygen atoms] is expected to yield a $^1A_1$ (**2**-C_{2v}) state of neutral Al_2O_3. Also, photodetaching an electron from the highest occupied b_2 and b_1 MOs should result in triplet and singlet combinations of the B_2 and B_1 states. Note that the b_2 and b_1 orbitals are in-plane and out-of-plane π-type bonding MOs on the terminal Al−O with large contributions from O-$2p_y$ and O-$2p_x$, respectively. The CCSD(T) results presented in Table 1, and discussed above, indicate that the energy separation between the $^3B_2$ and $^3B_1$ states of Al_2O_3 is small and that these triplet states are definitely lower in energy than the $^1A_1$ states of both **2**-C_{2v} and **3**-C_{2v}. Furthermore, the results in Table 3 show that the adiabatic electron detachment energies (AEDE) computed at the CCSD(T)/6-311+G(2df) level for the process ($^2A_1 \rightarrow {}^3B_2$; **2**-$C_{2v}$ structure) is 3.28 eV. This value is equivalent to the adiabatic electron affinity (AEA) for the lowest state of Al_2O_3 predicted by the theoretical model employed in this work. The AEA measured by Wang et al. from the PES experiment is 3.71 eV, resulting in a discrepancy of about 0.43 eV between theory and experiment. On the other hand, the vibrational frequency of 850 ± 80 cm^{-1} observed for the ground state of Al_2O_3 is in reasonable agreement with 925 cm^{-1} [(a_1 mode); not scaled] computed for the $^3B_2$ (**2**-C_{2v}) lowest electronic state at the B3LYP level (see Table 4). The source of the approximately 0.4 eV difference in our computed AEA and the observed value is not very clear to us. A theoretical AEA should be lower than the observed one partly because of the more difficult task of calculating an accurate total energy for the anion ground state. On the other hand, the level of theory employed in this work seems adequate for a reliable prediction of the AEA. Nonetheless, the following should be noted. The appearance of a broad ground-state X-band in the PES experiment[5] is consistent with the pronounced difference in the calculated geometries of the $^2A_1$ (**2**-C_{2v}) and $^3B_2$ (**2**-C_{2v}) lowest states of the anion and neutral species, respectively. For example, the terminal Al−O distance (R_c) is lengthened by 0.093 Å (MP2) and 0.10 Å (B3LYP) on going from $^2A_1$ (**2**-C_{2v}) to $^3B_2$ (**2**-C_{2v}) because of the removal of an electron from the highest occupied b_2 in-plane π-type bonding MO of the anion. Accordingly, the Al−O stretching (a_1 mode) is lowered from 1030 cm^{-1} in $^2A_1$ (**2**-C_{2v}) to 925 cm^{-1} in $^3B_2$ (**2**-C_{2v}). Furthermore, since the energy separation between the lowest lying triplet states of Al_2O_3 is small, these states may appear as overlapping bands, thereby contributing to the broadening of the photoelectron spectrum. Perhaps a properly resolved and better quality spectrum in future work will help resolve this slight discrepancy in computed and observed AEA of Al_2O_3.

A thorough study has been carried out on the **1**-$D_{\infty h}$ linear isomer of Al_2O_3. Therefore, a discussion of its structure and harmonic vibrational frequencies[2,4] will not be repeated here. It is important to note, however, that **1**-$D_{\infty h}$ is unstable for $Al_2O_3^-$ and that it can distort to the **5**-C_{2v} local minimum. Electron detachment from the stable "W-shaped" **5**-C_{2v} of the anion to give the neutral linear structure will result in considerable broadening of the photoelectron spectrum because of the significant change in geometry. Furthermore, the AEDE of 2.20 eV computed at the CCSD(T)/6-311+G(2df) level for the $^2A_1$

TABLE 2: Geometries (Å, deg) of Al_2O_3 and $Al_2O_3^-$ Computed at the MP2 and B3LYP Levels with the 6-311+G(2df) Basis Set

	structure	state	R_a	R_b	R_c	R_d	θ_e	θ_f
				Al_2O_3				
MP2	**1**-$D_{\infty h}$	$^1\Sigma_g^+$	1.683	1.621				
	2-C_{2v}	$^1A_1$	1.671	1.928	1.630	2.417	86.9	105.0
		$^3B_2$	1.766	1.743	1.741	2.406	94.3	92.6
		$^3B_1$	1.765	1.746	1.748	2.411	93.9	92.6
	3-C_{2v}	$^1A_1$	1.768		1.661	2.412	94.0	
		$^3B_2$	1.754		1.739	2.405	93.4	
		$^3B_1$	1.755		1.747	2.412	93.2	
	4-C_{2v}	$^1A_1$	1.712	1.728	1.672		57.7	
	6-D_{3h}	$^1A_1'$	2.576	1.807	2.052			
		$^3A_2'$	2.500	1.819	2.214			
CCSD(T)[a]	**1**-$D_{\infty h}$	$^1\Sigma_g^+$	1.689	1.620				
	2-C_{2v}	$^3B_2$	1.779	1.754	1.756	2.414	92.9	94.6
CCSD(T)[b]	**1**-$D_{\infty h}$	$^1\Sigma_g^+$	1.681	1.614				
	2-C_{2v}	$^3B_2$	1.768	1.744	1.743	2.409	92.6	94.2
B3LYP	**1**-$D_{\infty h}$	$^1\Sigma_g^+$	1.677	1.601				
	2-C_{2v}	$^1A_1$	1.676	1.862	1.620	2.407	87.9	100.9
		$^3B_2$	1.760	1.734	1.739	2.398	94.2	92.4
		$^3B_1$	1.758	1.737	1.749	2.405	93.8	92.3
	3-C_{2v}	$^1A_1$	1.752		1.633	2.402	93.4	
		$^3B_2$	1.752		1.738	2.399	93.3	
		$^3B_1$	1.747		1.748	2.406	93.0	
	4-C_{2v}	$^1A_1$	1.700	1.727	1.665		57.2	
	6-D_{3h}	$^1A_1'$	2.565	1.800	2.056			
		$^3A_2'$	2.481	1.805	2.198			
				$Al_2O_3^-$				
MP2	**1**-$D_{\infty h}$	$^2\Sigma_g^+$	1.702	1.640				
	2-C_{2v}	$^2A_1$	1.726	1.837	1.648	2.463	88.9	96.3
		$^2B_2$	1.876	1.714	1.771	2.474	98.4	87.6
	3-C_{2v}	$^2A_1$	1.776		1.652	2.459	92.4	
		$^2B_2$	1.780		1.768	2.456	92.7	
	4-C_{2v}	$^2B_1$	1.730	1.810	1.644		56.3	
	5-C_{2v}	$^2A_1$	1.735	1.639			103.5	152.8
	6-D_{3h}	$^2A_1'$	2.581	1.825	2.109			
B3LYP	**1**-$D_{\infty h}$	$^2\Sigma_g^+$	1.700	1.624				
	2-C_{2v}	$^2A_1$	1.723	1.821	1.635	2.453	89.1	95.8
	3-C_{2v}	$^2A_1$	1.768		1.640	2.454		92.1
	4-C_{2v}	$^2B_1$	1.718	1.803	1.639		55.9	
	5-C_{2v}	$^2A_1$	1.727	1.626			103.5	152.1
	6-D_{3h}	$^2A_1'$	2.570	1.821	2.110			

[a] CCSD(T)/6-31G(d). [b] CCSD(T)/6-311G(d).

TABLE 3: Adiabatic Electron Detachment Energies[a] (AEDE, eV) of $Al_2O_3^-$

structure	anion	neutral	method	AEDE
2-C_{2v}	$^2A_1$	$^1A_1$	CCSD(T)[b]	4.27
			CCSD(T)[c]	4.27
	$^2A_1$	$^3B_1$	CCSD(T)[b]	3.42
			CCSD(T)[c]	3.42
	$^2A_1$	$^3B_2$	CCSD(T)[b]	3.28
			CCSD(T)[c]	3.28
3-C_{2v}	$^2A_1$	$^1A_1$	CCSD(T)[b]	4.13
	$^2A_1$	$^3B_2$	CCSD(T)[b]	3.17
			CCSD(T)[c]	3.17

[a] In the photoelectron spectrum of $Al_2O_3^-$, two distinct bands are observed at binding energies of 3.71 and 4.32 eV. A third band at 4.9 eV is not definitely identified owing to background noise (see ref 5). The measured adiabatic electron affinity of Al_2O_3 is reported to be 3.71 ± 0.03 eV. [b] CCSD(T)/6-311+G(2df) computed at the MP2/6-311+G(2df) geometries. [c] CCSD(T)/6-311+G(2df) computed at the B3LYP/6-311+G(2df) geometries.

(**5**-C_{2v}) → $^1\Sigma_g^+$ (**1**-$D_{\infty h}$) process is inconsistent with the observed electron affinity. Thus, in agreement with the observation reported in ref 5, the linear structure can be ruled out as the species observed in the negative ion PES experiment.[5] For future studies on the Al_2O_3 molecule, the harmonic vibrational frequencies, including isotopic frequency shifts, are provided in Table 4 for the C_{2v} structures that have been found to be more stable than the linear isomer.

B. $Al_2O_2^-$ and Al_2O_2. The lowest energy structure computed for $Al_2O_2^-$ is a planar rhombus (nearly square) of D_{2h} symmetry, depicted as **1**-D_{2h} in Figure 2. Vibrational frequency analysis establishes **1**-D_{2h} ($^2B_{1u}$) as a minimum energy structure. Note that the molecular plane is the *yz* plane with the *z* axis along the shorter diagonal. By use of the B3LYP and MP2 optimized geometries, the linear form (**2**-$C_{\infty v}$, $^2\Sigma^+$) is computed to be 1.53 eV above **1**-D_{2h} ($^2B_{1u}$) at the CCSD(T) level. The harmonic vibrational frequencies calculated for the optimized geometry of **2**-$C_{\infty v}$ ($^2\Sigma^+$), however, possess one doubly degenerate imaginary frequency. Distortion of **2** leads to a **3**-C_s ($^2A'$) local minimum 1.1 eV above **1**-D_{2h} ($^2B_{1u}$). The $^2B_{2g}$ and $^2B_{3u}$ states of **1**-D_{2h} are predicted to be 2.25 and 2.26 eV, respectively, above the $^2B_{1u}$ state. Geometries and relative energies of the structures considered for $Al_2O_2^-$ are listed in Table 5. It may be concluded from these results that the ground state for the anion is the $^2B_{1u}$ state of **1**-D_{2h}.

The ground state of Al_2O_2 is found to be a ^1A_g state, also with a rhombic D_{2h} structure, in agreement with earlier theoretical predictions.[2,13] CCSD(T) places the linear form (**2**-$C_{\infty v}$, $^1\Sigma^+$) 0.37 eV above the ground state. The lowest triplet state ($^3B_{1u}$) is computed to be 0.47 eV above the ^1A_g ground state. Note the similarity in the geometries and the harmonic vibrational frequencies (see Table 6) of the excited $^3B_{1u}$ state and the ^1A_g ground state. The photoelectron spectrum of $Al_2O_2^-$ obtained by Wang and his collaborators is reported to show

TABLE 4: Harmonic Vibrational Frequencies for the 2-C_{2v} Structures of $Al_2O_3^-$ and Al_2O_3, and the 3-C_{2v} Isomer of $Al_2O_3^-$ [a]

	$Al_2O_3^-$ [**2**-C_{2v} ($^2A_1$)]			Al_2O_3 [**2**-C_{2v} ($^3B_2$)]			Al_2O_3 [**2**-C_{2v} ($^3B_1$)]		
	($Al_2{}^{16}O_3$)	($Al_2{}^{18}O_3$)	*R*(16/18)	($Al_2{}^{16}O_3$)	($Al_2{}^{18}O_3$)	*R*(16/18)	($Al_2{}^{16}O_3$)	($Al_2{}^{18}O_3$)	*R*(16/18)
a_1	1030 (168)	1000 (158)	1.0300	925 (172)	903 (163)	1.0244	911 (178)	890 (169)	1.0236
	805 (56)	771 (57)		753 (114)	721 (123)	1.0444	757 (132)	725 (134)	1.0441
	618 (84)	587 (69)		682 (76)	650 (55)		681 (56)	648 (40)	
	444 (1)	433 (0)		452 (1)	438 (0)		453 (0)	439 (0)	
b_1	355 (65)	346 (59)		353 (86)	342 (81)		349 (92)	338 (88)	
	161 (7)	156 (6)		140 (4)	137 (4)		142 (6)	138 (5)	
b_2	789 (137)	762 (126)	1.0354	776 (199)	749 (188)	1.0360	774 (194)	747 (182)	1.0361
	530 (47)	511 (45)		641 (16)	618 (14)		639 (8)	617 (7)	
	241 (27)	232 (23)		182 (16)	175 (14)		205 (10)	197 (10)	
ZPE	7.1			7.0			7.0		
	Al_2O_3 [**2**-C_{2v} ($^1A_1$)]			Al_2O_3 [**3**-C_{2v} ($^3B_2$)]			Al_2O_3 [**3**-C_{2v} ($^1A_1$)]		
	($Al_2{}^{16}O_3$)	($Al_2{}^{18}O_3$)	*R*(16/18)	($Al_2{}^{16}O_3$)	($Al_2{}^{18}O_3$)	*R*(16/18)	($Al_2{}^{16}O_3$)	($Al_2{}^{18}O_3$)	*R*(16/18)
a_1	1037 (8)	1006 (7)		915 (161)	894 (153)	1.0235	1015 (1)	987 (1)	
	862 (5)	824 (4)		775 (131)	743 (132)	1.0431	754 (1)	715 (1)	
	512 (2)	490 (2)		673 (66)	639 (50)		627 (20)	602 (17)	
	449 (2)	436 (2)		452 (0)	438 (0)		464 (2)	452 (2)	
b_1	372 (103)	360 (97)	1.0333	354 (86)	343 (82)		372 (96)	360 (92)	1.0333
	156 (1)	152 (1)		132 (4)	128 (3)		184 (4)	180 (4)	
b_2	902 (86)	871 (83)	1.0356	771 (216)	744 (203)	1.0363	740 (138)	714 (131)	1.0364
	446 (61)	430 (58)		646 (0)	624 (0)		636 (0)	613 (0)	
	237 (11)	228 (9)		181 (16)	174 (14)		241 (9)	232 (8)	
ZPE	7.1			7.0			7.1		

[a] Infrared intensities (in parentheses) are in km/mol and the zero-point vibrational energies (ZPE) are in kcal/mol. The isotopic frequency ratios *R*(16/18) are provided for the most intense IR bands. All calculations are carried out at the B3LYP/6-311+G(2df) level.

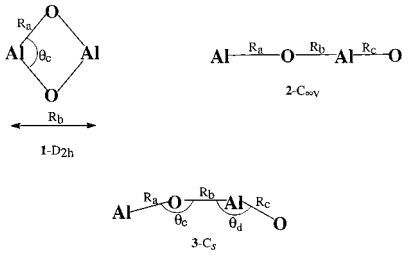

Figure 2. Structures of Al_2O_2 investigated in this work.

three bands labeled X, A, and B at binding energies of 1.88, 2.37, and 5.1 eV, respectively. The ground-state X-band of Al_2O_2 is reported to exhibit a vibrational progression with a frequency of 660 ± 80 cm^{-1}, while a frequency of 730 ± 80 cm^{-1} is recorded for the excited A state. An adiabatic electron affinity of 1.88 eV is measured for the ground state of Al_2O_2. The experimental data suggest that the excited states A and B lie 0.49 and 3.22 eV, respectively, above the ground state of the neutral species.

Our calculations predict the ground state of $Al_2O_2^-$ to be the $^2B_{1u}$ (**1**-D_{2h}) state. The valence electron orbital configuration is ... $(a_g)^2(b_{2u})^2(b_{1u})^2(a_g)^2(b_{3g})^2(b_{3u})^2(b_{1g})^2(b_{2u})^2$ $(a_g)^2(b_{1u})^1$. The ^1A_g ground state of Al_2O_2 (**1**-D_{2h}) can be formed by photodetaching an electron from the b_{1u} highest occupied MO (HOMO). Electron detachment from the highest occupied a_g, b_{2u}, $b_{1\,g}$, b_{3u} MOs yields excited singlet and triplet B_{1u}, B_{3g}, A_u, and B_{2g} states of **1**-D_{2h}. As presented in Table 5, the CCSD(T) adiabatic detachment energy (AEDE) for the $^2B_{1u}$ (**1**-D_{2h}) → ^1A_g (**1**-D_{2h}) process is 1.79 eV. Including the correction for the zero-point energy gives a value of 1.81 eV. The latter value corresponds to the calculated adiabatic electron affinity and compares well with the experimental value of 1.88 eV. The A state observed in the PES experiment is assigned to the excited $^3B_{1u}$ state computed to be 0.47 eV above the ^1A_g ground state of Al_2O_2. Again, the latter value agrees quite well with negative ion PES data[5] that places the lowest excited state of Al_2O_2 at 0.49 eV above the ground state. In addition, the observation of the ground-state X-band and the excited-state A-band as sharp peaks[5] is consistent with the similarity in the calculated geometries of the ^1A_g and $^3B_{1u}$ states of the neutral species and that of the $^2B_{1u}$ ground state of the anion (see Table 5). Finally, the observed vibrational progression with characteristic frequency of 660 ± 80 cm^{-1} for the ground state and 730 ± 80 cm^{-1} for the lowest excited state, compare reasonably with

TABLE 5: Geometries[a] (Å, deg) and Relative Energies (eV)[b,c] of Al_2O_2 and $Al_2O_2^-$

		MP2/6-311+G(2df)			CCSD(T)[d]	CCSD(T)[e]
structure	state	R_a	R_b	θ_c	ΔE	ΔE
			Al_2O_2			
2-$C_{\infty v}$	$^1\Sigma^+$	1.727	1.681		0.36	0.37
1-D_{2h}	$^3B_{3u}$	1.762	2.334	97.1	4.26	
1-D_{2h}	$^3B_{2g}$	1.755	2.397	93.9	4.02	
1-D_{2h}	^3A_u	1.822	2.724	83.2	3.09	
1-D_{2h}	$^3B_{3g}$	1.809	2.881	74.5	2.44	
1-D_{2h}	$^3B_{1u}$	1.763	2.422	93.2	0.46	0.47
1-D_{2h}	^1A_g	1.766	2.423	93.3	0.00 (1.79)	0.00 (1.79)
			$Al_2O_2^-$			
2-$C_{\infty v}$	$^2\Sigma^+$	1.694	1.746		(1.53)	(1.53)
3-C_s	$^2A'$	1.678	1.776		(1.10)	(1.11)
1-D_{2h}	$^2B_{1u}$	1.790	2.483	92.2	(0.00)	(0.00)

[a] B3LYP/6-311+G(2df) geometry for **1**-D_{2h} (^1A_g): R_a = 1.755 Å, R_b = 2.422 Å, θ_c = 92.8°. B3LYP/6-311+G(2df) geometry for **1**-D_{2h} ($^3B_{1u}$): R_a = 1.757 Å, R_b = 2.416 Å, θ_c = 93.1°. B3LYP/6-311+G(2df) geometry for **2**-$C_{\infty v}$ ($^1\Sigma^+$): R_a = 1.725 Å, R_b = 1.673 Å, R_c = 1.605 Å; R_c = 1.608 Å (MP2). B3LYP/6-311+G(2df) geometry for **1**-D_{2h} ($^2B_{1u}$): R_a = 1.779 Å, R_b = 2.481 Å, θ_c = 91.6°. B3LYP/6-311+G(2df) geometry for **2**-$C_{\infty v}$ ($^2\Sigma^+$): R_a = 1.688 Å, R_b = 1.749 Å, R_c = 1.637 Å; R_c = 1.632 Å (MP2). B3LYP/6-311+G(2df) geometry for **3**-C_s ($^2A'$): R_a = 1.673 Å, R_b = 1.769 Å, R_c = 1.647 Å, θ_c = 176.9°, θ_d = 130.7°. Also for for **3**-C_s ($^2A'$), R_c = 1.658 Å, θ_c = 161.7°, θ_d = 130.9° at the MP2 level. [b] Total energies (in hartrees) of Al_2O_2 and $Al_2O_2^-$. For **1**-D_{2h} (^1A_g): $E_{CCSD(T)//MP2}$ = −634.354 954; $E_{CCSD(T)//B3LYP}$ = −634.355 100. For **1**-D_{2h} ($^2B_{1u}$): $E_{CCSD(T)//MP2}$ = −634.420 818; $E_{CCSD(T)//B3LYP}$ = −634.420 849. [c] Values in parentheses are relative to the $^2B_{1u}$ ground state of $Al_2O_2^-$. [d] CCSD(T)/6-311+G(2df) computed at the MP2/6-311+G(2df) geometries (CCSD(T)//MP2). [e] CCSD(T)/6-311+G(2df) computed at the B3LYP/6-311+G(2df) geometries (CCSD(T)//B3LYP).

TABLE 6: Harmonic Vibrational Frequencies for the 1-D_{2h} Structures of $Al_2O_2^-$ and Al_2O_2[a]

	$Al_2O_2^-$ [**1**-D_{2h} ($^2B_{1u}$)]			Al_2O_2 [**1**-D_{2h} (^1A_g)]			Al_2O_2 [**1**-D_{2h} ($^3B_{1u}$)]		
	($Al_2{}^{16}O_2$)	($Al_2{}^{18}O_2$)	*R*(16/18)	($Al_2{}^{16}O_2$)	($Al_2{}^{18}O_2$)	*R*(16/18)	($Al_2{}^{16}O_2$)	($Al_2{}^{18}O_2$)	*R*(16/18)
a_g	740	708		790	756		774	743	
	485	477		513	505		518	508	
b_{3g}	571	551		621	600		614	593	
b_{1u}	514 (189)	496 (180)	1.0363	554 (91)	534 (84)	1.0374	729 (329)	703 (306)	1.0370
b_{2u}	693 (118)	668 (106)	1.0374	757 (164)	730 (153)	1.0370	730 (148)	704 (138)	1.0369
b_{3u}	260	251		307 (40)	296 (37)		283 (20)	273 (18)	
ZPE	4.7			5.1			5.2		

[a] Infrared intensities (in parentheses) are in km/mol and the zero-point vibrational energies (ZPE) are in kcal/mol. The isotopic frequency ratios *R*(16/18) are provided for the most intense IR bands. All calculations are carried out at the B3LYP/6-311+G(2df) level.

B3LYP values (unscaled) of 790 and 774 cm^{-1} for the a_g mode of the ^1A_g ground state and $^3B_{1u}$ lowest excited state, respectively.

Concluding Remarks

The lowest energy structure computed for the Al_2O_3 molecule is the C_{2v} structure labeled **2**-C_{2v} in Figure 1. The **2**-C_{2v} ($^3B_2$) structure is roughly 7 kcal/mol more stable than the linear **1**-$D_{\infty h}$ ($^1\Sigma_g^+$) structure previously identified in cryogenic matrix studies. However, according to our calculations, **1**-$D_{\infty h}$ ($^1\Sigma_g^+$) is the lowest energy structure on the singlet potential energy surface, in agreement with previous theoretical studies.[2,3] The adiabatic electron affinity calculated for the **2**-C_{2v} ($^3B_2$) structure of Al_2O_3 at the CCSD(T) level differs from the value obtained from PES by roughly 0.4 eV. We suggest that a reevaluation of the experimental data may be in order.

In the case of Al_2O_2, the results confirm the **1**-D_{2h} structure as the most stable. Our calculations suggest that the ^1A_g ground state is about 0.47 eV below the lowest triplet state ($^3B_{1u}$). This singlet−triplet (S−T) energy separation is in very good agreement with experimental PES results for $Al_2O_2^-$, which place the lowest excited state of Al_2O_2 at 0.49 eV above the ground state. The adiabatic electron affinity, including the correction for the zero-point energy, is calculated to be 1.81 eV for Al_2O_2. The latter value is in good agreement with the experimental value of 1.88 eV.

Finally, it should be remarked that to date, none of the "rhombic like" D_{2h} structures, theoretically predicted as the most stable forms of Al_2O_x (x = 2, 3, 4) have been definitely identified in matrix isolation studies. Only the linear isomers of these species have been observed and characterized for Al_2O_2 and Al_2O_3.[4] The recent photoelectron experiments, however, appear to support theoretical predictions that find the D_{2h} forms to be the lowest energy structures. We hope that the data presented in this and earlier[15] work will assist future experimental studies on Al_2O_3 and Al_2O_4.

Acknowledgment. We thank the Natural Sciences and Engineering Research Council of Canada and the University of Ottawa for financial support. We also thank the Mississippi Center for Supercomputing Research for a generous allocation of computer time.

References and Notes

(1) Solomonik, V. G.; Sliznev, V. V. *Russ. J. Inorg. Chem.* **1987**, *32*, 788 (transl. of *Zh. Neor. Khim.*).
(2) Nemukhin, A. V.; Weinhold, F. *J. Chem. Phys.* **1992**, *97*, 3420.
(3) Rozhanskii, I. L.; Serebrennikov, L. V.; Shevel'kov, A. F. *Russ. J. Phys. Chem.* **1990**, *64*, 276 (transl. of *Zh. Fiz. Khim.*).
(4) Andrews, L.; Burkholder, T. R.; Yustein, J. T. *J. Phys. Chem.* **1992**, *96*, 10182.
(5) Desai, S. R.; Wu, H.; Rohlfing, C. M.; Wang, L. S. *J. Chem. Phys.* **1997**, *106*, 1309.
(6) Marino, C. P.; White, D. *J. Phys. Chem.* **1973**, *77*, 2929.
(7) Finn, P. A.; Gruen, D. M.; Page, D. L. *Adv. Chem. Ser.* **1976**, *158*, 30.
(8) Serebrennikov, L. V.; Osin, S. B.; Maltsev, A. A. *J. Mol. Struct.* **1982**, *81*, 25.
(9) Sonchik, S. M.; Andrews, L.; Carlson, K. D. *J. Phys. Chem.* **1983**, *87*, 2004.
(10) Rozhanskii, I. L.; Chertikhin, G. V.; Serebrennikov, L. V.; Shevel'kov, V. F. *Russ. J. Phys. Chem.* **1988**, *62*, 1215 (Transl. of *Zh. Fiz. Khim.*).
(11) Bencivenni, L.; Pelino, M.; Ramondo, F. *J. Mol. Struct.: THEOCHEM* **1992**, *253*, 109.
(12) Zaitsevskii, A. V.; Chertihin, G. V.; Serebrennikov, L. V.; Stepanov, N. F. *J. Mol. Struct.*: *THEOCHEM* **1993**, *280*, 291
(13) Archibong, E. F.; Sullivan, R. H. *J. Phys. Chem.* **1995**, *99*, 15830.
(14) Archibong, E. F.; St-Amant, A. *Chem. Phys. Lett.* **1998**, *284*, 331.
(15) Archibong, E. F.; St-Amant, A. *J. Phys. Chem. A* **1998**, *102*, 6877.
(16) Hehre, W. J.; Radom, L.; Schleyer, P. v. R.; Pople, J. A. *Ab Initio Molecular Orbital Theory*; Wiley: New York, 1986.
(17) Frish, M. J.; Trucks, G. W.; Schlegel, H. B.; Gill, P. M. W.; Johnson, B. G.; Robb, M. A.; Cheeseman, J. R.; Keith, T. A.; Peterson, G. A.; Montgomery, J. A.; Raghavachari, K.; Al-Laham, M. A.; Zakrzewski, V. G.; Ortiz, J. V.; Foresman, J. B.; Cioslowski, J.; Stefanov, B. B.; Nanayakkara, A.; Challacombe, M.; Peng, C. Y.; Ayala, P. Y.; Chen, W.; Wong, M. W.; Andres, J. L.; Replogle, E. S.; Gomperts, R.; Martin, R. L.; Fox, D. J.; Binkley, J. S.; DeFrees, D. J.; Baker, J.; Stewart, J. P.; Head-Gordon, M.; Gonzalez, C.; Pople, J. A. *GAUSSIAN 94*; Gaussian, Inc.: Pittsburgh, PA, 1995.